

Selection rules for electromagnetic transitions in triaxially deformed odd- A nuclei

Kosai Tanabe*

*Theoretical Nuclear Physics Laboratory, RIKEN Nishina Center, Wako, Saitama 351-0198, Japan and
Department of Physics, Saitama University, Sakura-Ku, Saitama 338-8570, Japan*

Kazuko Sugawara-Tanabe†

Otsuma Women's University, Tama, Tokyo 206-8540, Japan

(Received 7 March 2008; published 23 June 2008)

The approximate selection rules for the interband and intraband electromagnetic transitions are predicted referring to two quantum numbers, which are derived from an algebraic solution for the particle-rotor model with one high- j nucleon coupled to a triaxially deformed core. It is shown that the inclusion of angular momentum dependence for moments of inertia reproduces the experimental excitation energies relative to a reference quite well both for positive and negative parity TSD bands in $^{161,163,165,167}\text{Lu}$.

DOI: 10.1103/PhysRevC.77.064318

PACS number(s): 21.10.Re, 21.60.Ev, 23.20.Lv, 27.70.+q

I. INTRODUCTION

In our previous paper [1] (to be referred to in what follows as I), it has been shown that the particle-rotor model with rigid-body moments of inertia consistently reproduces details of the experimental energy level schemes as well as the electromagnetic transition rates for the triaxially strongly deformed (TSD) bands in odd- A Lu isotopes [2–5]. In I, we extended the Holstein-Primakoff (HP) transformation for the rotor Hamiltonian in the even nucleus [6] to the case of the odd-mass nucleus by introducing two kinds of bosons for the total angular momentum \vec{I} and the single-particle angular momentum \vec{j} . Then, we can obtain the precise algebraic solution by taking into account the invariance of the nuclear states under Bohr symmetry group [7]. The algebraic treatment allows an automatic introduction of two kinds of quantum numbers describing precessions of \vec{I} and \vec{j} . In this scheme, both angular momenta interact on an equal footing, and the precession of the core angular momentum $\vec{R} = \vec{I} - \vec{j}$ correlates with that of \vec{j} . Such an interplay between two tops with \vec{R} and \vec{j} is called the “top-on-top mechanism”. As for ^{163}Lu , similar mechanism is also discussed by Hamamoto in a somewhat different way [8].

The HP transformation is also applicable to the electromagnetic transition rates. The selection rules are inferred from the lowest-order overlaps between the eigenstates of the algebraic solution and the Fock space in the original HP bosons. Since there have been observed many TSD bands in Lu and Hf isotopes [9], whose angular momenta are not yet determined experimentally, the approximate selection rules become useful to identify the angular momenta and the precession quantum numbers of these bands.

As is shown in I, the energy level scheme with the rigid-body moments of inertia differs from that with the hydrodynamical moments of inertia even when the sign of γ is so chosen as to reproduce the length of three axes in the same

order as in the rigid-body. The purpose of the present paper is, at first, to derive the selection rules for the electromagnetic transitions from the viewpoints of the quantum numbers classifying yrast and yrare favored and unfavored bands, and of their energy level schemes depending on the models.

The second purpose of the present paper is to reproduce the detailed behavior of energy levels, that is represented by the excitation energy relative to a reference, i.e., $E^* - aI(I+1)$ with $a = 0.0075$ MeV. Increase of the dynamical moments of inertia even at larger I in the TSD bands is attributed to the gradual collapse of the pairing in the rotating core moments of inertia. We simulate the decrease of pairing effect by a gradual increase of the core moments of inertia as a function of I , and apply the formula to both positive and negative parity TSD bands in Lu isotopes, i.e., ^{161}Lu [10], ^{163}Lu [2,3,9], ^{165}Lu [4], and ^{167}Lu [5].

In Sec. II, we briefly review our algebraic formalism [1], and discuss the difference in the level order between the rigid-body moments of inertia and the hydrodynamical moments of inertia based on the quantum numbers introduced by the algebraic solution. In Sec. III, the selection rules are derived from the approximate algebraic expressions of the matrix elements for the interband and intraband transitions. In Sec. IV, the theoretical results including an angular momentum dependence for moments of inertia are compared with experimental energy levels relative to a reference. In Sec. V, the paper is concluded.

II. FORMALISM

The particle-rotor Hamiltonian is given by

$$H = H_{\text{rot}} + H_{\text{sp}} \quad (1)$$

with

$$H_{\text{rot}} = \sum_{k=x,y,z} A_k (I_k - j_k)^2, \quad (2a)$$

$$H_{\text{sp}} = \frac{V}{j(j+1)} [\cos \gamma (3j_z^2 - \vec{j}^2) - \sqrt{3} \sin \gamma (j_x^2 - j_y^2)], \quad (2b)$$

*kosai@muj.biglobe.ne.jp

†tanabe@otsuma.ac.jp

where $A_k = 1/(2\mathcal{J}_k)$ ($k = 1, 2, 3$ or x, y, z). We adopt the rigid-body model in Lund convention,

$$\mathcal{J}_k^{\text{rig}} = \frac{\mathcal{J}_0}{1 + \left(\frac{5}{16\pi}\right)^{1/2} \beta_2} \left[1 - \left(\frac{5}{4\pi}\right)^{1/2} \beta_2 \cos\left(\gamma + \frac{2}{3}\pi k\right) \right], \quad (3)$$

where (β_2, γ) are the deformation parameters describing ellipsoidal shape of the rotor. The maximum moment of inertia is about x -axis and the relation $\mathcal{J}_x^{\text{rig}} \geq \mathcal{J}_y^{\text{rig}} \geq \mathcal{J}_z^{\text{rig}}$ holds in the range of $0 \leq \gamma \leq 2\pi/3$. The sign of γ in H_{sp} is chosen so that the oscillator strength is the largest in the x -direction in consistent with the largest $\mathcal{J}_x^{\text{rig}}$. For comparison we adopt the hydrodynamical moments of inertia in Copenhagen convention [12], where $\mathcal{J}_x^{\text{hyd}} \geq \mathcal{J}_y^{\text{hyd}} \geq \mathcal{J}_z^{\text{hyd}}$ holds in the range of $0 \leq \gamma \leq \pi/3$,

$$\mathcal{J}_k^{\text{hyd}} = \frac{4}{3} \mathcal{J}_0 \sin^2\left(\gamma - \frac{2}{3}\pi k\right). \quad (4)$$

The factors in Eqs. (3) and (4) are chosen so that $\mathcal{J}_x^{\text{hyd}} = \mathcal{J}_x^{\text{rig}} = \mathcal{J}_0$ at $\gamma = 0$. Note that a common value of the scaling factor $s = \mathcal{J}_0 V$ yields the same physical contents except for energy scale.

We must pay special attention to the important symmetry properties of the nuclear Hamiltonian and the nuclear state, i.e., D_2 symmetry group and Bohr symmetry group [7,12] (the invariance under both symmetry operations will be referred to simply as the D_2 -invariance, hereafter). Now we consider the case where x -axis is chosen as a quantization axis, and then a complete set of the D_2 -invariant basis is given by

$$\left[\sqrt{\frac{2I+1}{16\pi^2}} [\mathcal{D}_{MK}^I(\theta_i) \phi_{\Omega}^j + (-1)^{I-j} \mathcal{D}_{M-K}^I(\theta_i) \phi_{-\Omega}^j]; \right. \\ \left. |K - \Omega| = \text{even}, \quad \Omega > 0 \right], \quad (5)$$

where K and Ω denote eigenvalues of I_x and j_x , respectively. The wave function ϕ_{Ω}^j stands for spherical basis for the single-particle state, and $\mathcal{D}_{MK}^I(\theta_i)$ Wigner \mathcal{D} -function. The magnitude R of the rotor angular momentum $\vec{R} = \vec{I} + (-\vec{j})$ is restricted to $R = |I - j|, |I - j| + 1, \dots, I + j - 1$, or $I + j$, so that an integer $n_{\beta'}$ defined by $R = I - j + n_{\beta'}$ ranges as

$$n_{\beta'} = 0, 1, 2, \dots, 2j - 1, \text{ or } 2j. \quad (6)$$

Since R_x runs from R to $-R$, and $R_x = I_x - j_x = K - \Omega = \text{even}$, an integer $n_{\alpha'}$ defined by the relation $R_x = R - n_{\alpha'}$ ranges as

$$\begin{aligned} n_{\alpha'} &= 0, 2, 4, \dots, \text{ or } 2R, & \text{for } R = \text{even}, \\ n_{\alpha'} &= 1, 3, 5, \dots, \text{ or } 2R - 1, & \text{for } R = \text{odd}. \end{aligned} \quad (7)$$

Thus, for a physical state which is described by a set of non-negative integers $(n_{\alpha'}, n_{\beta'})$, the magnitude of rotor angular momentum R and its x -component R_x are given by $R = I - j + n_{\beta'}$ and $R_x = I - j + n_{\beta'} - n_{\alpha'}$ as a result of the D_2 -invariance requirement.

As shown by the present authors 37 years ago [6], the higher order terms in the HP boson expansion should be included

to reproduce the rotational spectra of the triaxially deformed rotor of an even nucleus. This is also the case for the odd- A nucleus which is discussed explicitly in I in association with the recovery of the D_2 -invariance. Since the moments of inertia \mathcal{J}_x is the largest, and therefore the coefficient of I_x^2 and j_x^2 are the smallest among the other coefficients in Eqs. (2a) and (2b), the total energy is expected to be the lowest when both angular momentum vectors \vec{I} and \vec{j} are aligned to the x -direction. Thus, we choose diagonal forms for the components I_x and j_x in the HP boson representation as follows:

$$\begin{aligned} I_+ &= I_-^\dagger = I_y + iI_z = -\hat{a}^\dagger \sqrt{2I - \hat{n}_a}, \\ I_x &= I - \hat{n}_a \quad \text{with } \hat{n}_a = \hat{a}^\dagger \hat{a}; \end{aligned} \quad (8a)$$

$$\begin{aligned} j_+ &= j_-^\dagger = j_y + ij_z = \sqrt{2j - \hat{n}_b} \hat{b}, \\ j_x &= j - \hat{n}_b \quad \text{with } \hat{n}_b = \hat{b}^\dagger \hat{b}. \end{aligned} \quad (8b)$$

Applying these HP representations to the Hamiltonian (1), we expand $\sqrt{2I - \hat{n}_a}$ and $\sqrt{2j - \hat{n}_b}$ into series in $\hat{n}_a/(2I)$ and $\hat{n}_b/(2j)$, and retain up to the next to leading order. We obtain

$$H_B = H_0 + H_2 + H_4, \quad (9)$$

where H_0 denotes a constant which collects all the terms independent of boson operators, H_2 the bilinear forms of boson operators, and H_4 the fourth order terms. The explicit definition of these terms are given in I. Diagonalization of H_2 is attained by the boson Bogoliubov transformation connecting boson operators $(\hat{a}, \hat{b}, \hat{a}^\dagger, \hat{b}^\dagger)$ to quasiboson operators $(\alpha, \beta, \alpha^\dagger, \beta^\dagger)$. Thus, the particle-rotor Hamiltonian is approximately expressed in terms of two kinds of quantum numbers as

$$\begin{aligned} H_B &= H_0 + \omega_\alpha + \omega_\beta + C_0 + (2\omega_\alpha + C_\alpha) \hat{n}_\alpha \\ &\quad + (2\omega_\beta + C_\beta) \hat{n}_\beta + C_{\alpha\alpha} \hat{n}_\alpha^2 + C_{\beta\beta} \hat{n}_\beta^2 + C_{\alpha\beta} \hat{n}_\alpha \hat{n}_\beta, \end{aligned} \quad (10)$$

where we introduce number operators in the new quasiparticle picture,

$$\hat{n}_\alpha = \alpha^\dagger \alpha \quad \text{and} \quad \hat{n}_\beta = \beta^\dagger \beta. \quad (11)$$

When there is no single-particle potential, i.e., $V = 0$ in Eq. (1), the formula (10) is reduced to a simple expression of the rotational energy with two quantum numbers, n_α and n_β , which are the eigenvalues of \hat{n}_α and \hat{n}_β ,

$$\begin{aligned} E_{\text{rot}}(I, n_\alpha, n_\beta) &= A_x R(R+1) - \frac{p+q}{2} n_\alpha^2 \\ &\quad + \left(2R\sqrt{pq} + \sqrt{pq} - \frac{p+q}{2} \right) \left(n_\alpha + \frac{1}{2} \right), \end{aligned} \quad (12)$$

where $p = A_y - A_x$, $q = A_z - A_x$ and $R = I - j + n_\beta$. Since, in the symmetric limit of $A_y = A_z$, the formula (12) goes to well-known expression $E_{\text{rot}}(I, n_\alpha, n_\beta) = A_z R(R+1) - (A_z - A_x)(R - n_\alpha)^2$, the eigenvalue R can be regarded as an effective magnitude of the rotor angular momentum, and $R - n_\alpha$ as its x -component R_x . It turns out that these n_α and n_β are the same integers $n_{\alpha'}$ and $n_{\beta'}$ as defined in Eqs. (6) and (7). This allows us to interpret the quantum number n_α as the ‘‘precession’’ of \vec{R} (so-called ‘‘wobbling’’ in the text book

of Bohr and Mottelson (BM) [12]) because of $R_x = R - n_\alpha$, and the quantum number n_β is interpreted as the ‘‘precession’’ of \vec{j} about the intrinsic x -axis because of Eq. (8b). Due to the mixing of bosons \hat{a} and \hat{b} , the physical contents of \hat{n}_α and \hat{n}_β change, but they keep the same eigenvalues as in the symmetric limit whole through the adiabatic change of interaction parameter V and deformation parameters (β_2, γ) . Thus, the rotational bands can be classified in terms of a pair of quantum numbers (n_α, n_β) which is restricted by the D_2 -invariance as in Eqs. (6) and (7). Here we comment that Eq. (12) has physical meaning except for the limit of $\gamma = 0$ (i.e., $p = 0$), where the transformation coefficients from the (α, β) picture to the (a, b) picture diverge [see Eq. (44c) in I].

The expression of Eq. (12) is useful to get a rough idea of the relative position in energy among different TSD bands. For instance, a contrast between \mathcal{J}^{rig} and \mathcal{J}^{hyd} for the case of large s is found in the difference between yrast energies of $(I, 0, 0)$ and $(I - 1, 1, 0)$:

$$\begin{aligned} E_{\text{rot}}(I - 1, 1, 0) - E_{\text{rot}}(I, 0, 0) \\ = 2(I - j)(\sqrt{pq} - A_x) - 2\sqrt{pq} - (p + q). \end{aligned} \quad (13)$$

In the limit of $\gamma = 0$ where $A_x = A_y$, Eq. (13) reduces to $-2(I - j)A_x - (A_z - A_x)$, which is negative, and $E_{\text{rot}}(I - 1, 1, 0)$ is smaller than $E_{\text{rot}}(I, 0, 0)$. On the other hand, in the limit where $A_y = A_z$, which appears at $\gamma = 30^\circ$ for \mathcal{J}^{hyd} and at $\gamma = 60^\circ$ for \mathcal{J}^{rig} , Eq. (13) reduces to $2(I - j)(A_z - 2A_x) - 4(A_z - A_x)$, which becomes positive under the conditions of $I \gg j$ and $A_z > 2A_x$. As \mathcal{J}^{hyd} changes more rapidly with γ than \mathcal{J}^{rig} , the condition of $A_z > 2A_x$ is satisfied by \mathcal{J}^{hyd} around $\gamma \sim 20^\circ$. Thus, the energy level of $(I - 1, 1, 0)$ is located higher than the one of $(I, 0, 0)$ for \mathcal{J}^{hyd} . On the other hand, around the region of $\gamma \sim 20^\circ$ which is far from 60° , \mathcal{J}^{rig} gives negative value of $\sqrt{pq} - A_x$, consequently the level of $(I - 1, 1, 0)$ is located lower than the one of $(I, 0, 0)$. This situation is not altered in the exact results (see Figs. 3 and 4 in I). Experimental data over Lu isotopes supports the levels with $I - 1$ in TSD2 band is lower than those with I in TSD1 band for $I > 45/2$.

Now we compare the energy difference between yrast band level of $(I, 2, 0)$ and the yrast band level of $(I, 0, 0)$ (ΔE_2) to the energy difference between the average of levels of $(I - 1, 1, 0)$ and $(I + 1, 1, 0)$ and the yrast band of $(I, 0, 0)$ (ΔE_1):

$$\begin{aligned} \Delta E_2 = E_{\text{rot}}(I, 2, 0) - E_{\text{rot}}(I, 0, 0) \\ = 4(I - j)\sqrt{pq} + 2\sqrt{pq} - 3(p + q), \end{aligned} \quad (14a)$$

$$\begin{aligned} \Delta E_1 = \frac{E_{\text{rot}}(I + 1, 1, 0) + E_{\text{rot}}(I - 1, 1, 0)}{2} - E_{\text{rot}}(I, 0, 0) \\ = 2(I - j)\sqrt{pq} + \sqrt{pq} - (p + q) + A_x. \end{aligned} \quad (14b)$$

It is seen from Eq. (14) that $2\Delta E_1 - \Delta E_2 = A_y + A_z$, which gives a measure of what is called anharmonicity, i.e., the deviation from the simple phonon approximation.

III. THE SELECTION RULES OF $E2$ AND $M1$ TRANSITION RATES

Diagonalization of H in Eq. (1) is carried out on the complete set of D_2 -invariant bases with the same form as given by Eq. (5), but K and Ω denote the eigenvalues of I_z and j_z , respectively. The $E2$ and $M1$ transition operators are given by

$$\begin{aligned} \mathcal{M}(E2, \mu) &= \sqrt{\frac{5}{16\pi}} e [Q_0 \mathcal{D}_{\mu 0}^2 + Q_2 (\mathcal{D}_{\mu 2}^2 + \mathcal{D}_{\mu -2}^2)], \\ \mathcal{M}(M1, \mu) &= \sqrt{\frac{3}{4\pi}} \mu_N \sum_{v=0, \pm 1} [(g_\ell - g_R) j_v \\ &\quad + (g_s - g_\ell) s_v + g_R I_v] \mathcal{D}_{\mu v}^1, \end{aligned} \quad (15)$$

where $\mu_N = e\hbar/(2Mc)$, g_ℓ is the orbital g -factor, g_s the spin g -factor, g_R the effective g -factor for the rotational motion. The components of the intrinsic quadrupole moments, i.e., Q_0 and Q_2 are related with the deformation parameter γ through the relation,

$$\frac{Q_2}{Q_0} = -\frac{\tan \gamma}{\sqrt{2}}, \quad (16)$$

which is consistent with the definition of \mathcal{J}^{rig} and H_{sp} in Eqs. (3) and (2b).

In the practice of numerical analysis, the $B(E2)$ and $B(M1)$ values for the intraband and interband transitions among various TSD bands can be directly calculated from the exact solutions to the Hamiltonian as already done in I. Now, our interest is in the selection rules to pick up expected linking transitions with stronger probabilities from various allowed transition modes among the TSD bands, whose relative positions in energy depend on either the rigid-body, or the hydrodynamical model. For this purpose, we refer to a pair of the quantum numbers (n_α, n_β) introduced by the algebraic solution. We need the transformation coefficients between two boson Fock spaces, i.e., the one is generated on the quasivacuum $|0\rangle_\alpha$ for quasibosons (α, β) and the other on the vacuum $|0\rangle_a$ for HP bosons (\hat{a}, \hat{b}) . Defining these overlaps is an extension of the coefficient G_{kl} [6,13,14] to the case with two kinds of boson. Such a set of the coefficients is calculated by applying the extended form of the generalized Wick theorem [15]. The eigenstates of H_B in Eq. (9) are expressed in terms of quasiboson numbers n_α and n_β together with I and j ,

$$|n_\alpha n_\beta, Ij\rangle = \frac{1}{\sqrt{n_\alpha! n_\beta!}} (\alpha^\dagger)^{n_\alpha} (\beta^\dagger)^{n_\beta} |0\rangle_\alpha. \quad (17)$$

Then, we consider the overlap between $|n_\alpha n_\beta, Ij\rangle$ and $|n_\alpha n_\beta, Ij\rangle$,

$$\begin{aligned} G_{n_\alpha n_\beta; n_\alpha n_\beta}^{Ij} &\equiv \frac{{}_a\langle 0 | \hat{a}^{n_\alpha} \hat{b}^{n_\beta} (\alpha^\dagger)^{n_\alpha} (\beta^\dagger)^{n_\beta} |0\rangle_\alpha}{(n_\alpha! n_\beta! n_\alpha! n_\beta!)^{1/2}} \\ &= \frac{{}_a\langle 0 | 0\rangle_\alpha}{(n_\alpha! n_\beta! n_\alpha! n_\beta!)^{1/2}} {}_a\langle 0 | \hat{a}^{n_\alpha} \hat{b}^{n_\beta} (\hat{O}) (\alpha^\dagger)^{n_\alpha} (\beta^\dagger)^{n_\beta} |0\rangle_\alpha \end{aligned} \quad (18)$$

with $(\hat{O}) \equiv 1/{}_a\langle 0 | 0\rangle_\alpha$. In this expression $n_\alpha (= I - K)$ and $n_\beta (= j - \Omega)$ stand for the eigenvalues of \hat{n}_a and \hat{n}_b ,

respectively. We notice that $G_{n_a, n_b; n_\alpha, n_\beta}^{Ij}$ is non-vanishing only when an integral value of $\Delta n \equiv n_a + n_b - n_\alpha - n_\beta$ is even. The value of $G_{n_a, n_b; n_\alpha, n_\beta}^{Ij}$ becomes 1 for $n_a = n_\alpha$ and $n_b = n_\beta$ only when, for the limit of $I \gg j$, $A_y = A_z$ for \mathcal{J}^{rig} ($\gamma = 60^\circ$), and an additional condition $V = 0$ is necessary for \mathcal{J}^{hyd} ($\gamma = 30^\circ$).

As discussed below Eq. (51) in I, an application of the generalized Wick theorem reduces the expectation value of the r.h.s. of Eq. (18) to a sum over $(n_a + n_b + n_\alpha + n_\beta - 1)!!$ terms, which are products of $(n_a + n_b + n_\alpha + n_\beta)/2$ factors from

$$\begin{aligned} A_{\mu\nu} &\equiv {}_a\langle 0 | (\hat{O}) \alpha_\mu^\dagger \alpha_\nu^\dagger | 0 \rangle_\alpha, & B_{\mu\nu} &\equiv {}_a\langle 0 | \hat{a}_\mu \hat{a}_\nu (\hat{O}) | 0 \rangle_{\hat{a}}, \\ C_{\mu\nu} &\equiv {}_a\langle 0 | \hat{a}_\mu (\hat{O}) \alpha_\nu^\dagger | 0 \rangle_\alpha, \end{aligned} \quad (19)$$

where the operator \hat{a}_μ represents either $\hat{a}_1 \equiv \hat{a}$ or $\hat{a}_2 \equiv \hat{b}$, and $\hat{\alpha}_1 \equiv \hat{\alpha}$ or $\hat{\alpha}_2 \equiv \hat{\beta}$. When the boson Bogoliubov transformation is in the vicinity of an identity transformation, the matrix C in Eq. (19) has finite diagonal elements, while elements of the other matrices A and B are vanishingly small. Therefore, in the realistic case, the matrix elements of A and B are expected to be smaller in comparison with those of C . For the case of $\Delta n \neq 0$, $G_{n_a, n_b; n_\alpha, n_\beta}^{Ij}$ gains A and/or B as extra factors. For simplicity, we employ an asymptotic estimation by assuming that I is large enough and the difference in the I -dependence of $G_{n_a, n_b; n_\alpha, n_\beta}^{Ij}$ between the initial and the final states is negligible. We drop indices I and j from $G_{n_a, n_b; n_\alpha, n_\beta}^{Ij}$, and employ its abbreviation as $G_{n_a, n_b; n_\alpha, n_\beta}$.

In order to investigate how the Coriolis coupling affects the wave function, we derive an explicit expression of $G_{n_a, n_b; n_\alpha, n_\beta}$ for the case of $V = 0$ from the algebraic solution leading to the energy expression Eq. (12) in the last section. Then, the Bogoliubov transformation connecting HP boson operators ($\hat{a}, \hat{b}, \hat{a}^\dagger, \hat{b}^\dagger$) to quasiboson operators ($\alpha, \beta, \alpha^\dagger, \beta^\dagger$) expressed in the form of Eq. (C1) in I is given by

$$\begin{pmatrix} \alpha \\ \beta \\ \alpha^\dagger \\ \beta^\dagger \end{pmatrix} = \begin{pmatrix} K & N \\ M & L \end{pmatrix} \begin{pmatrix} \hat{a} \\ \hat{b} \\ \hat{a}^\dagger \\ \hat{b}^\dagger \end{pmatrix}, \quad (20)$$

where the submatrices are

$$K = L = \begin{pmatrix} \left(\frac{I}{I-j}\right)^{1/2} \eta_+ & -\left(\frac{j}{I-j}\right)^{1/2} \eta_- \\ 0 & \left(\frac{I}{I-j}\right)^{1/2} \end{pmatrix}, \quad (21a)$$

$$M = N = \begin{pmatrix} -\left(\frac{I}{I-j}\right)^{1/2} \eta_- & \left(\frac{j}{I-j}\right)^{1/2} \eta_+ \\ \left(\frac{j}{I-j}\right)^{1/2} & 0 \end{pmatrix} \quad (21b)$$

with

$$\eta_\pm = \left\{ \frac{1}{\text{sgn}(p-q)} \right\} \left[\frac{1}{2} \left(\frac{p+q}{2\sqrt{pq}} \pm 1 \right) \right]^{1/2}. \quad (22)$$

Hence, the matrices defined in Eq. (19) become

$$A = MK^{-1} = \begin{pmatrix} -\frac{\eta_-}{\eta_+} & \left(\frac{j}{I}\right)^{1/2} \frac{1}{\eta_+} \\ \left(\frac{j}{I}\right)^{1/2} \frac{1}{\eta_+} & \frac{j\eta_-}{I\eta_+} \end{pmatrix}, \quad (23a)$$

$$B = -K^{-1}N = \begin{pmatrix} \frac{\eta_-}{\eta_+} \frac{I-j}{I} & -\left(\frac{j}{I}\right)^{1/2} \\ -\left(\frac{j}{I}\right)^{1/2} & 0 \end{pmatrix}, \quad (23b)$$

$$C = K^{-1} = \begin{pmatrix} \left(\frac{I-j}{I}\right)^{1/2} \frac{1}{\eta_+} & \left(\frac{I-j}{I}\right)^{1/2} \left(\frac{j}{I}\right)^{1/2} \frac{\eta_-}{\eta_+} \\ 0 & \left(\frac{I-j}{I}\right)^{1/2} \end{pmatrix}. \quad (23c)$$

Using Eq. (23), we obtain, for example, $\Delta n = 0$ diagonal elements of G

$$G_{0000} = \frac{1}{\sqrt{\det K}} = \left(\frac{I-j}{I}\right)^{1/2} \frac{1}{\eta_+^{1/2}}, \quad (24a)$$

$$G_{1010} = G_{0000} C_{11} = \frac{I-j}{I} \frac{1}{\eta_+^{3/2}}, \quad (24b)$$

$$\begin{aligned} G_{2020} &= \frac{G_{0000}}{2!} (A_{11} B_{11} + 2C_{11} C_{11}) \\ &= \left(\frac{I-j}{I}\right)^{3/2} \frac{1}{\eta_+^{5/2}} \left(1 - \frac{\eta_-^2}{2}\right); \end{aligned} \quad (24c)$$

and $\Delta n = 0$ nondiagonal elements

$$G_{1001} = G_{0000} C_{12} = \frac{I-j}{I} \left(\frac{j}{I}\right)^{1/2} \frac{\eta_-}{\eta_+^{3/2}}, \quad (25a)$$

$$\begin{aligned} G_{1120} &= \frac{G_{0000}}{\sqrt{2!}} (A_{11} B_{12} + 2C_{11} C_{21}) \\ &= \left(\frac{I-j}{I}\right)^{1/2} \left(\frac{j}{I}\right)^{1/2} \frac{\eta_-}{\eta_+^{3/2}}. \end{aligned} \quad (25b)$$

As for $|\Delta n| = 2$ elements we obtain, for example,

$$G_{2000} = \frac{G_{0000}}{\sqrt{2!}} B_{11} = \frac{1}{\sqrt{2}} \left(\frac{I-j}{I}\right)^{3/2} \frac{\eta_-}{\eta_+^{3/2}}, \quad (26a)$$

$$G_{1100} = G_{0000} B_{12} = -\left(\frac{I-j}{I}\right)^{1/2} \left(\frac{j}{I}\right)^{1/2} \frac{1}{\eta_+^{1/2}}, \quad (26b)$$

$$\begin{aligned} G_{2101} &= \frac{G_{0000}}{\sqrt{2!}} (B_{11} C_{22} + 2B_{12} C_{12}) \\ &= \frac{1}{\sqrt{2}} \frac{I-j}{I} \frac{I-3j}{I} \frac{\eta_-}{\eta_+^{3/2}}. \end{aligned} \quad (26c)$$

The factors $\sqrt{(I-j)/I}$ and $\sqrt{j/I}$ arise from the effect of the Coriolis terms and the recoil terms, which are not included in the case of BM. The factors of $\sqrt{j/I}$ and η_- together with the increasing power in $\sqrt{(I-j)/I}$ reduce the contributions to the transition rates from non-diagonal elements of G with $\Delta n = 0$ and $\Delta n \neq 0$ digits. This implies that the “ $\Delta n = 0$ ” approximation works even better for the TSD bands in odd- A nuclei than in even mass case. We remark that, only if we put $j = 0$, $G_{n_a, n_b; n_\alpha, n_\beta}$ with the digits

TABLE I. The $B(E2)$ value for the transition from the initial state of I to the final state of $I - 2$ among the bands with quantum numbers (n_α, n_β) within “ $\Delta n = 0$ ” approximation. The common factor of $5e^2/(16\pi)$ is abbreviated. The higher order contribution of $\Delta n \neq 0$ is denoted by “h.o.,” and “-” represents that there is no level in the final states due to D_2 -invariance. Further details are in the text.

Final $I - 2$	Initial I				
	(0, 0)	(1, 0)	(2, 0)	(3, 0)	(0, 1)
(0, 0)	$(Q'_2 G_{0000})^2$	-	$\frac{3}{7^2} (Q'_0 G_{0000} G_{2020})^2$	-	-
(1, 0)	-	$(Q'_2 G_{1010})^2$	-	$\frac{9}{7^2} (Q'_0 G_{3030} G_{1010})^2$	$[Q'_2 (G_{0101} G_{0110} + G_{1010} G_{1001})]^2$
(2, 0)	h.o.	-	$(Q'_2 G_{2020})^2$	-	-
(3, 0)	-	h.o.	-	$(Q'_2 G_{3030})^2$	h.o.
(0, 1)	-	$[Q'_2 (G_{0101} G_{0110} + G_{1010} G_{1001})]^2$	-	$\frac{3}{7^2} [Q'_0 (\sqrt{3} G_{3030} G_{1001} + G_{0101} G_{2130})]^2$	$(Q'_2 G_{0101})^2$

$n_b = n_\beta = 0$ reduces to $G_{n_\alpha n_\alpha}$ [6,13,14], which is comparable with the case of “wobbling” in BM [12]. Needless to say that $M1$ transition is beyond the scope of the BM formalism, which does not include a valence nucleon coupled to the core.

An approximation collecting only a few terms of $G_{n_\alpha n_\beta n_\alpha n_\beta}$ in the lowest order is useful to derive selection rules, and to estimate the order of magnitude of the transition matrix elements. Since our interest is in the TSD bands with small n 's, we choose an approximation taking only terms with $G_{n_\alpha n_\beta n_\alpha n_\beta}$ whose digits satisfy $\Delta n = 0$. As an example of realistic calculation, we have compared the “ $\Delta n = 0$ ” approximation and the “ $\Delta n = 2$ ” approximation with the exact results for the $B(E2)$ and $B(M1)$ values in Table I in I. We found that the “ $\Delta n = 0$ ” approximation simulates the exact results reasonably well.

Associated with the change of quantization axis from z - to x -axis, the components of quadrupole moment must be transformed to

$$\begin{cases} Q_0 \\ Q_2 \end{cases} \rightarrow \begin{cases} Q'_0 = -\frac{1}{2} Q_0 (1 + \sqrt{3} \tan \gamma) \\ Q'_2 = \frac{1}{2\sqrt{2}} Q_0 (\sqrt{3} - \tan \gamma), \end{cases} \quad (27)$$

where we have used Eq. (16). In the algebraic treatment, Q_0 and Q_2 in Eq. (15) must be replaced by Q'_0 and Q'_2 , respectively, and the algebraic expressions for $B(E2)$ and $B(M1)$ are given by Eqs. (57) and (58) in I.

The reduced $E2$ transition rates $B(E2)$ are summarized in Tables I to IV. Table I is for the transition from the initial states of I to the final ones of $I - 2$, Table II is to the final states of $I - 1$, and Table III is to the final states of I . Similarly, the approximate reduced $M1$ transition rates $B(M1)$ are summarized in Table IV for the transition from the initial states of I to the final ones of $I - 1$, and in Table V to the final states of I . The precession quantum numbers (n_α, n_β) assigned to the initial states of I are given in the second row starting from the second column, while those assigned to the final states are given in the first column in each table. The bands with (0, 0) and (1, 0) are the yrast bands, and those with (2, 0) and (3, 0) are the yrare bands for the case of \mathcal{J}^{rig} , while those with (2, 0) and (0, 1) are the yrare bands for the case of \mathcal{J}^{hyd} with large s (see Figs. 3 and 4 in I). As for the positive parity bands in Lu isotopes, the yrast favored band has (0, 0) and the yrast unfavored band has (1, 0), as $j = 13/2$ is assumed. In Tables I, II, and IV, “h.o.” represents that the dominant contribution starts from the higher order terms of $|\Delta n| = 2$, or 4. In all tables, “-” represents that no level exists in the final state by the D_2 -invariance. For simplicity, we abbreviated the common factors $5e^2/(16\pi)$ from $B(E2)$ and $3(\mu_N g_{\text{eff}})^2/(16\pi)$ with $g_{\text{eff}} \equiv g_\ell + (g_s - g_\ell)/(2j)$ from $B(M1)$. Needless to say, the diagonal elements of $B(E2)$ for $\Delta I = 0$ transitions in Table III, and those of $B(M1)$ in Table V are not transition rates, but are related with the square of static moments. The elements in the diagonal position in Table I are related with

TABLE II. The $B(E2)$ value for the transition from the initial state of I to the final state of $I - 1$ among the bands with quantum numbers (n_α, n_β) within “ $\Delta n = 0$ ” approximation. The common factor of $5e^2/(16\pi)$ is abbreviated. The symbols are the same as defined in Table I.

Final $I - 1$	Initial I				
	(0, 0)	(1, 0)	(2, 0)	(3, 0)	(0, 1)
(0, 0)	-	$\frac{3}{7} (Q'_0 G_{0000} G_{1010})^2$	-	$\frac{3}{7^3} (Q'_2 G_{0000} G_{3030})^2$	$\frac{3}{7} (Q'_0 G_{0000} G_{1001})^2$
(1, 0)	$\frac{2}{7} (Q'_2 G_{0000} G_{1010})^2$	-	$\frac{6}{7} (Q'_0 G_{2020} G_{1010})^2$	-	-
(2, 0)	-	$\frac{4}{7} (Q'_2 G_{2020} G_{1010})^2$	-	$\frac{9}{7} (Q'_0 G_{2020} G_{3030})^2$	$\frac{2}{7} [Q'_2 (\sqrt{2} G_{2020} G_{1001} + G_{0101} G_{1120})]^2$
(3, 0)	h.o.	-	$\frac{6}{7} (Q'_2 G_{3030} G_{2020})^2$	-	-
(0, 1)	$\frac{2}{7} (Q'_2 G_{0000} G_{1001})^2$	-	$\frac{3}{7} [Q'_0 (\sqrt{2} G_{2020} G_{1001} + G_{0101} G_{1120})]^2$	-	-

TABLE III. The $B(E2)$ value for the transition from the initial state of I to the final state of I among the bands with quantum numbers (n_α, n_β) within “ $\Delta n = 0$ ” approximation. The common factor of $5e^2/(16\pi)$ is abbreviated. The symbols are the same as defined in Table I. The diagonal matrix elements are not transition rates, but related with the static quadrupole moments.

Final I	Initial I				
	(0, 0)	(1, 0)	(2, 0)	(3, 0)	(0, 1)
(0, 0)	$(Q'_0 G_{0000})^2$	–	$\frac{3}{I^2} (Q'_2 G_{0000} G_{2020})^2$	–	–
(1, 0)	–	$(Q'_0 G_{1010})^2$	–	$\frac{9}{I^2} (Q'_2 G_{3030} G_{1010})^2$	$[Q'_0 (G_{0101} G_{0110} + G_{1010} G_{1001})]^2$
(2, 0)	$\frac{3}{I^2} (Q'_2 G_{2020} G_{0000})^2$	–	$(Q'_0 G_{2020})^2$	–	–
(3, 0)	–	$\frac{9}{I^2} (Q'_2 G_{3030} G_{1010})^2$	–	$(Q'_0 G_{3030})^2$	$\frac{3}{I^2} [Q'_2 (\sqrt{3} G_{3030} G_{1001} + G_{0101} G_{2130})]^2$
(0, 1)	–	$[Q'_0 (G_{0101} G_{0110} + G_{1010} G_{1001})]^2$	–	$\frac{3}{I^2} [Q'_2 (\sqrt{3} G_{3030} G_{1001} + G_{0101} G_{2130})]^2$	$(Q'_0 G_{0101})^2$

intraband or inband transition $B(E2)_{in}$. All the other transition rates in nondiagonal positions in all Tables correspond to inter-band or out-of-band transitions, i.e., $B(E2)_{out}$ and $B(M1)_{out}$.

Using the approximate formulas for the transition rates given in Tables I and II, we show that the $B(E2)_{out}$ values for the $|\Delta I| = 2$ transition from TSD3 (2, 0) to TSD1 (0,0), and for the $|\Delta I| = 1$ transition to TSD1 (1,0) are reproduced from the known $|\Delta I| = 1$ transition from TSD2 (1,0) to TSD1 (0,0) in ^{163}Lu . Experimental $B(E2)_{out}/B(E2)_{in}$ values for the $|\Delta I| = 1$ transition from TSD3 to TSD2 are around 0.51 ± 0.13 at $I = 45/2$, from TSD2 to TSD1 are around 0.2 for $I = 37/2 \sim 57/2$, and $|\Delta I| = 2$ transition from TSD3 to TSD1 are around 0.02 for $I = 37/2 \sim 57/2$ [3]. The $|\Delta I| = 1$ transition from TSD2 (1,0) to TSD1 (0,0) are well explained in terms of our model as demonstrated in I. The following relations are derived from Tables I and II:

$$\frac{B(E2; I, 10 \rightarrow I - 1, 00)}{B(E2; I, 10 \rightarrow I - 2, 10)} \sim \frac{3}{I} \left(\frac{Q'_0 G_{0000}}{Q'_2 G_{1010}} \right)^2, \quad (28)$$

$$\frac{B(E2; I, 20 \rightarrow I - 2, 00)}{B(E2; I, 20 \rightarrow I - 2, 20)} \sim \frac{3}{I^2} \left(\frac{Q'_0 G_{0000}}{Q'_2 G_{2020}} \right)^2, \quad (29)$$

$$\frac{B(E2; I, 20 \rightarrow I - 1, 10)}{B(E2; I, 20 \rightarrow I - 2, 20)} \sim \frac{6}{I} \left(\frac{Q'_0 G_{1010}}{Q'_2 G_{2020}} \right)^2. \quad (30)$$

Thus, putting 0.2 in the l.h.s. of Eq. (28), we proceed with the estimation as follows:

$$\begin{aligned} \text{[r.h.s. of Eq. (29)]} &= \frac{1}{I} \left(\frac{G_{1010}}{G_{2020}} \right)^2 \times \text{[r.h.s. of Eq. (28)]} \\ &\sim \frac{0.2}{I} \sim 0.01, \end{aligned} \quad (31)$$

which is comparable with the experimental value of 0.02. Similarly, we get

$$\begin{aligned} \text{[r.h.s. of Eq. (30)]} &= 2 \left(\frac{G_{1010}^2}{G_{0000} G_{2020}} \right)^2 \times \text{[r.h.s. of Eq. (28)]} \\ &\sim 2 \times 0.2 = 0.4, \end{aligned} \quad (32)$$

which is also comparable with the experimental value of 0.51 ± 0.13 . Experimental $B(M1)_{out}/B(E2)_{in}$ value from TSD3 to TSD2 is around $0.006^{+0.006}_{-0.004} (\mu_N^2/e^2 b^2)$ at $I = 51/2$ [3]. This value is also related to the experimental value from TSD2 to TSD1 for $I = 35/2 \sim 51/2$, $B(M1)_{out}/B(E2)_{in} \sim 0.006$ [2], which is well explained in terms of our model as presented in I. The following relations are derived from Tables I and IV:

$$\frac{B(M1; I, 10 \rightarrow I - 1, 00)}{B(E2; I, 10 \rightarrow I - 2, 10)} = \frac{3(\mu_N g_{eff})^2}{5(eQ'_2)^2} \frac{4j^2}{I} \left(\frac{G_{0000}}{G_{1010}} \right)^2, \quad (33)$$

TABLE IV. The $B(M1)$ value for the transition from the initial state of I to the final state of $I - 1$ among the bands with quantum numbers (n_α, n_β) within “ $\Delta n = 0$ ” approximation. The common factor of $3(\mu_N g_{eff})^2/(16\pi)$ is abbreviated. The symbols are the same as defined in Table I.

Final $I - 1$	Initial I				
	(0, 0)	(1, 0)	(2, 0)	(3, 0)	(0, 1)
(0, 0)	–	$\frac{4j^2}{I} (G_{0000} G_{1010})^2$	–	$\frac{2j}{I^2} (G_{0000} G_{2130})^2$	$\frac{4j^2}{I} (G_{0000} G_{1001})^2$
(1, 0)	$4j (G_{0000} G_{0110})^2$	–	$\frac{8j^2}{I} (G_{2020} G_{1010})^2$	–	–
(2, 0)	–	$4j (G_{1120} G_{1010})^2$	–	$\frac{12j^2}{I} (G_{2020} G_{3030})^2$	$8j (G_{0220} G_{0101})^2$
(3, 0)	h.o.	–	$4j (G_{2130} G_{2020})^2$	–	–
(0, 1)	$4j (G_{0000} G_{0101})^2$	–	$\frac{4j^2}{I} (G_{2020} G_{1001} + G_{0101} G_{1120})^2$	–	–

TABLE V. The $B(M1)$ value for the transition from the initial state of I to the final state of I among the bands with quantum numbers (n_α, n_β) within “ $\Delta n = 0$ ” approximation. The common factor of $3(\mu_N g_{\text{eff}})^2/(16\pi)$ is abbreviated. The definition of the symbols is the same as defined in Table I. The diagonal matrix elements are not transition rates, but related with the static magnetic moments.

Final I	Initial I				
	(0, 0)	(1, 0)	(2, 0)	(3, 0)	(0, 1)
(0, 0)	$(2jG_{0000})^2$	–	$\frac{4j}{I}(G_{0000}G_{1120})^2$	–	–
(1, 0)	–	$(2jG_{1010})^2$	–	$\frac{8j}{I}(G_{1010}G_{2130})^2$	$[2j(G_{1010}G_{1001} + G_{0101}G_{0110})]^2$
(2, 0)	$\frac{4j}{I}(G_{0000}G_{1120})^2$	–	$(2jG_{2020})^2$	–	–
(3, 0)	–	$\frac{8j}{I}(G_{1010}G_{2130})^2$	–	$(2jG_{3030})^2$	$\frac{8j}{I}(G_{0101}G_{1230})^2$
(0, 1)	–	$[2j(G_{1010}G_{1001} + G_{0101}G_{0110})]^2$	–	$\frac{8j}{I}(G_{0101}G_{1230})^2$	$(2jG_{0101})^2$

$$\frac{B(M1; I, 20 \rightarrow I - 1, 10)}{B(E2; I, 20 \rightarrow I - 2, 20)} = \frac{3(\mu_N g_{\text{eff}})^2 8j^2}{5(eQ_2')^2} \frac{8j^2}{I} \left(\frac{G_{1010}}{G_{2020}} \right)^2. \quad (34)$$

Thus, putting 0.006 in the l.h.s. of Eq. (33), we proceed to the estimation as follows:

$$\begin{aligned} [\text{r.h.s. of Eq. (34)}] &= 2 \left(\frac{G_{1010}^2}{G_{0000}G_{2020}} \right)^2 \times [\text{r.h.s. of Eq. (33)}] \\ &\sim 2 \times 0.006 = 0.012, \end{aligned} \quad (35)$$

which is comparable with the experimental value of $0.006_{-0.004}^{+0.006}$. In the above estimates, we have assumed the diagonal elements of G as 1, i.e., $G_{mnmn} \sim 1$. This approximation is well justified by the numerical analysis employing \mathcal{J}^{rig} and the same set of parameters as in Figs. 1 to 4 (as for the parameters, see the subsequent paragraph). The result gives $G_{0000} \sim 0.96$, $G_{1010} \sim 0.92$, $G_{2020} \sim 0.85$ and $G_{3030} \sim 0.81$ for $I = 39/2 \sim 59/2$. For comparison, the nondiagonal elements of G , which are referred to within “ $\Delta n = 0$ ” approximation, are given by $G_{1001} \sim 0.09$, $G_{0110} \sim -0.02$, $G_{1120} \sim -0.05$, $G_{0220} \sim -0.03$, and $G_{2130} \sim 0.03$, whose magnitudes are much smaller than those of diagonal elements. In addition, some $|\Delta n| = 2$ values of G are given by $G_{2000} = 0.15$, $G_{3001} = 0.03$, $G_{1100} = -0.16$ and $G_{2101} = 0.12$. These values are much smaller than the $\Delta n = 0$ diagonal elements.

In order to clarify the difference between the rigid-body model and the hydrodynamical model, we show the approximate $B(E2)_{\text{out}}$ and $B(M1)_{\text{out}}$ values together with the energy level scheme specific to each model. The order of energy levels through low-lying four bands is based on the results of the exact diagonalization of H in Eq. (1) with $s = 120$, $\mathcal{J}_0 = 52.4 \text{ MeV}^{-1}$, $\gamma = 17^\circ$ and $\beta = 0.38$ at $I = 53/2$ both for \mathcal{J}^{rig} (Figs. 1 and 2), and \mathcal{J}^{hyd} (Figs. 3 and 4). The initial and the final levels are specified by attached angular momenta, and the quantum numbers (n_α, n_β) below each band. We show the schematic figure of $B(E2)_{\text{out}}$ without the common factor of $5e^2/(16\pi)$ in Figs. 1 and 3, and $B(M1)_{\text{out}}$ transitions without the common factor of $3(\mu_N g_{\text{eff}})^2/(16\pi)$ in Figs. 2 and 4. Since our interest is in comparing the orders of strength among competing transitions, we have replaced the diagonal elements G_{mnmn} by 1 in both B values in all figures. In Figs. 1 and 2,

we show a level of I belonging to the favored yrast band with (0, 0), two levels of $I \pm 1$ belonging to each of the unfavored yrast band with (1, 0) and the unfavored yrare band with (3, 0), and two levels of I and $I + 2$ belonging to the favored yrare band with (2, 0). Similarly, in Figs. 3 and 4, we show a level of I belonging to the favored yrast band with (0, 0), a level of I belonging to the yrare band with (2, 0), and two levels of $I \pm 1$ belonging to each of the unfavored yrast band with (1, 0) and the unfavored yrare bands with (0, 1).

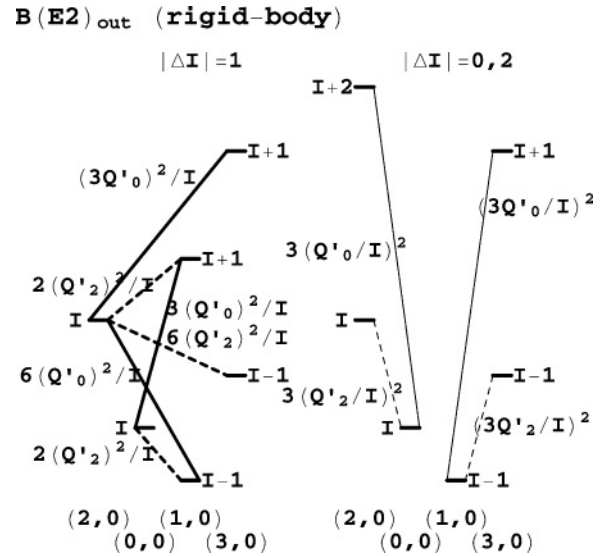


FIG. 1. The $E2$ transition schemes with \mathcal{J}^{rig} and the $B(E2)_{\text{out}}$ values estimated from “ $\Delta n = 0$ ” and “ $G_{mnmn} = 1$ ” approximation. The left panel is for $|\Delta I| = 1$, and the right panel is for $|\Delta I| = 0$ and 2 interband $E2$ transitions. In each panel, the quantum numbers assigned to each band (n_α, n_β) are shown underneath the typical band levels of I or $I - 1$. The energy scale in the vertical direction is arbitrary, but the energy differences are proportional to the exact results obtained from the total Hamiltonian. The $B(E2)_{\text{out}}$ values without a common factor $5e^2/(16\pi)$ are given beside the lines of allowed transitions. According to their strength, the transitions are classified by strong (thick solid), less strong (thick dashed), weak (thin solid) and weaker (thin dashed) lines. Further details are in the text.

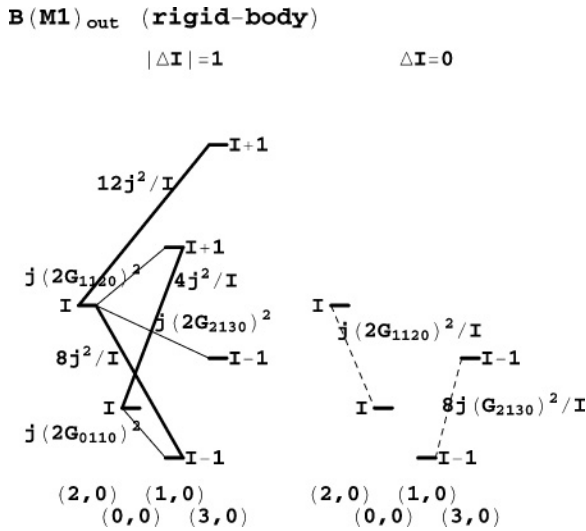


FIG. 2. The $M1$ transition schemes with \mathcal{J}^{rig} and the $B(M1)_{\text{out}}$ values estimated from “ $\Delta n = 0$ ” and “ $G_{mnmn} = 1$ ” approximation. The left panel is for $|\Delta I| = 1$, and the right panel is for $\Delta I = 0$ interband $M1$ transitions. The definition of symbols and the energy scale are the same as in Fig. 1. The $B(M1)_{\text{out}}$ values without a common factor $3(\mu_N g_{\text{eff}})^2/(16\pi)$ are shown beside the lines of allowed transitions. The transitions are classified with the same kinds of lines as in Fig. 1. Further details are in the text.

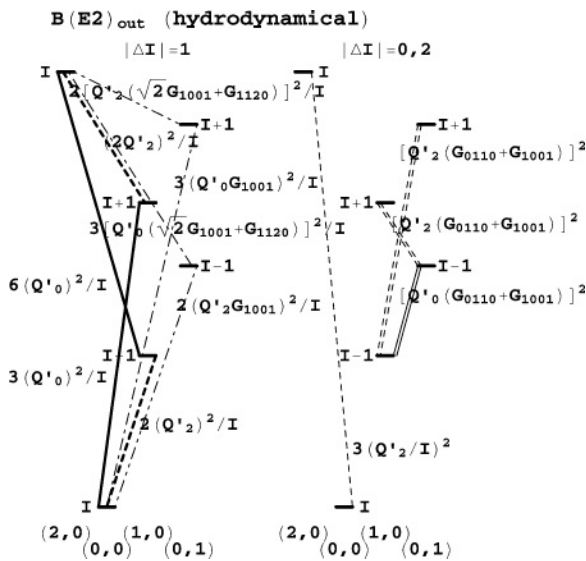


FIG. 3. The $E2$ transition schemes with \mathcal{J}^{hyd} and the $B(E2)_{\text{out}}$ values estimated from “ $\Delta n = 0$ ” and “ $G_{mnmn} = 1$ ” approximation. The left panel is for $|\Delta I| = 1$, and the right panel is for $|\Delta I| = 0$ and 2 interband $E2$ transitions. The definition of symbols is the same as employed in Fig. 1. The energy scale in the vertical direction is arbitrary, but the energy differences are proportional to the exact results obtained from the total Hamiltonian. According to the strength, the transitions are classified by strong (thick solid), less strong (thick dashed), weak (thin dashed), weaker (dot-dashed) and weakest (double-dot-dashed) lines. Special transitions independent of the factor $1/I$ are indicated by strong (double solid) and less strong (double dashed) lines. Further details are in the text.

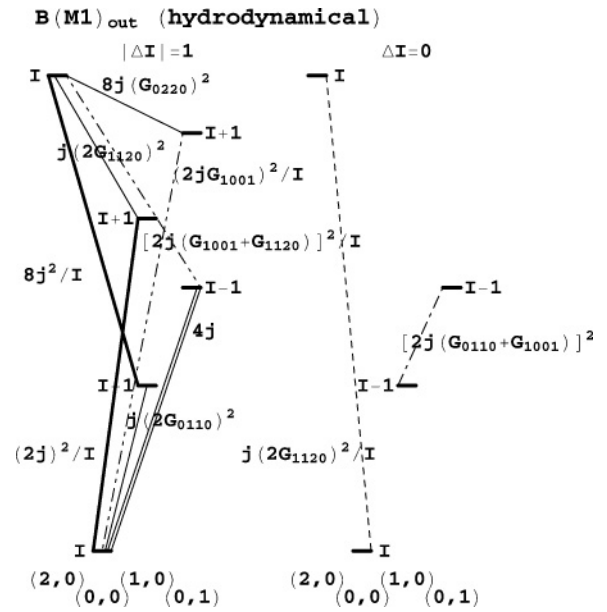


FIG. 4. The $M1$ transition schemes with \mathcal{J}^{hyd} and the $B(M1)_{\text{out}}$ values estimated from “ $\Delta n = 0$ ” and “ $G_{mnmn} = 1$ ” approximation. The left panel is for $|\Delta I| = 1$, and the right panel is for $\Delta I = 0$ interband $M1$ transitions. The definition of symbols and the energy scale are the same as in Fig. 3. The $B(M1)_{\text{out}}$ values without a common factor $3(\mu_N g_{\text{eff}})^2/(16\pi)$ are shown beside the lines of allowed transitions. According to their strength, the transition are classified by strong (thick solid), less strong (dot-dashed), weak (double-dot-dashed), weaker (thin solid) and weakest (thin dashed) lines. A special transition independent of the factor $1/I$ and non-diagonal element of G is indicated by double solid lines. Further details are in the text.

As for the $B(E2)_{\text{out}}$ values in Figs. 1 and 3, their magnitudes are controlled by three factors as follows. (1) All the $B(E2)_{\text{out}}$ values depend on either Q'_0 or Q'_2 , and $(Q'_0)^2$ is larger than $(Q'_2)^2$ for $\gamma > 0^\circ$ as is seen in Eqs. (27). (2) The magnitudes of the nondiagonal elements $|G_{n_a n_b n_a n_b}|$ ($n_a \neq n_a$, and/or $n_b \neq n_b$) are much smaller than the diagonal elements $G_{mnmn} (\sim 1)$. (3) The $B(E2)_{\text{out}}$ values with a factor $1/I^2$ is much smaller than those with $1/I$ for large I . Based on these rules, the strong transition rate $(Q'_0)^2/I$ is denoted by thick solid line, the next $(Q'_2)^2/I$ by thick dashed line, the third $(Q'_0/I)^2$ by thin solid line and the last $(Q'_2/I)^2$ is by thin dashed line. As is seen in Fig. 1, for example, the transition rate from the excited unfavored band level of $(I + 1, 1, 0)$ to the favored band level of $(I, 0, 0)$ is $3(Q'_0)^2/I$ and denoted by thick solid line. While the transition from the favored band level of $(I, 0, 0)$ to the unfavored band level of $(I - 1, 1, 0)$ is $2(Q'_2)^2/I$, which is weaker than the former and denoted by thick dashed line. This staggering behavior of the transition is seen in Fig. 8 in I. All the transitions in the right panel is smaller than those in the left panel due to the factor $1/I^2$.

In Figs. 2 and 4, the $B(M1)_{\text{out}}$ values obey the rules: (1) Compared with the order of j/I which is about 0.25, the square of the non-diagonal elements of G 's are smaller, for example, $(G_{1001})^2 \sim 0.008$ and $(G_{0110})^2 \sim 0.0004$. (2) $1/I^2$ is smaller than $1/I$. Based on these rules, the strong transition j^2/I is denoted by thick solid line, the next $j(G_{0110})^2$ by thin

solid line, the third $j(G_{0110})^2/I$ by thin dashed line in Fig. 2. As is seen in the left panel of Fig. 2, the transition from the yrare unfavored band level of $(I + 1, 1, 0)$ to the yrast favored band level of $(I, 0, 0)$ is denoted by thick solid line, while the transition from $(I, 0, 0)$ to $(I - 1, 1, 0)$ is denoted by thin solid line. This staggering is seen in Fig. 8 in I.

In Figs. 3 and 4, we show the case of \mathcal{J}^{hyd} , where the favored yrast, yrare and unfavored yrast bands have the same quantum numbers as in the case of \mathcal{J}^{rig} , but the yrare unfavored band have the quantum numbers $(0, 1)$ instead of $(3, 0)$. Although the quantum numbers of the yrast favored and the unfavored bands are the same both for \mathcal{J}^{rig} and \mathcal{J}^{hyd} , a contrast between them is seen in the level order, as is discussed based on Eq. (13) in Sec. II. The yrast favored band level of $(I, 0, 0)$ is located lower than the yrast unfavored band level of $(I - 1, 1, 0)$. Thus, there appear the transitions not only from I to $I - 1$, but also from I to $I + 1$, which do not appear in Figs. 1 and 2 for \mathcal{J}^{rig} . For example, the level of $(I, 2, 0)$ decays not only to the $I - 1$ level, but also to $I + 1$ levels with $(1, 0)$ and with $(0, 1)$, as is seen in the left panel of Fig. 3. The $|\Delta I| = 2$ transitions between $(0, 1)$ and $(1, 0)$ bands appear without $1/I$ factor in the right panel of Fig. 3. Thus, in addition to the transitions in Fig. 1, new types of transitions appear, i.e., the transition rates of $(Q'_0 G_{1001})^2/I$ and $[Q'_0(\sqrt{2}G_{1001} + G_{1120})]^2/I$ denoted by dot-dashed lines, and those of $[Q'_2(\sqrt{2}G_{1001} + G_{1120})]^2/I$ and $(Q'_2 G_{1001})^2/I$ by double-dot-dashed line. In the right panel of Fig. 3, the transition of $[Q'_0(G_{1001} + G_{0110})]^2$ is denoted by double solid lines, and that of $[Q'_2(G_{1001} + G_{0110})]^2$ by double dashed lines. These transition rates do not have explicit I -dependence, though the nondiagonal G 's depend weakly on I , so that they keep almost constant even for large I . As is shown in Fig. 3, the transition rate from the level of $(I + 1, 1, 0)$ to the level of $(I, 0, 0)$ is the same $3(Q'_0)^2/I$ as in Fig. 1, but the transition from the level of $(I, 0, 0)$ to the level of $(I - 1, 1, 0)$ never exists in the deexcitation process, since the level of $(I - 1, 1, 0)$ is located higher than the level of $(I, 0, 0)$. As for the $|\Delta I| = 2$ interband transitions, there is the transition from $(I + 2, 2, 0)$ to $(I, 0, 0)$ with the same transition rate $3(Q'_0/I)^2$ as in the right panel of Fig. 1, though it is not shown in the right panel of Fig. 3.

Similarly, new types of $M1$ -transitions appear in Fig. 4, because of the difference between the cases of \mathcal{J}^{rig} and \mathcal{J}^{hyd} . As is seen in the right panel of Fig. 4, the $\Delta I = 0$ transition rate between $(0, 1)$ and $(1, 0)$ bands is in the order of j^2 multiplied by the square of nondiagonal G 's, so that it keeps almost constant independent of I , which is denoted by dot-dashed line. In the left panel of Fig. 4, the transitions from the level of $(I + 1, 0, 1)$ to $(I, 0, 0)$, and from the level of $(I, 2, 0)$ to $(I - 1, 0, 1)$ are denoted by double-dot-dashed lines, since they gain an extra factor $1/I$ in comparison with the transition denoted by dot-dashed line in the right panel. Another special type of transition from $(I - 1, 0, 1)$ to $(I, 0, 0)$ is found in the left panel of Fig. 4. Its transition rate is in the order of $4j$ independent of I , and is denoted by double solid line. The transition rate from the level of $(I + 1, 1, 0)$ to $(I, 0, 0)$ is $4j^2/I$ which is the same as in Fig. 2, but the transition from the level of $(I, 0, 0)$ to $(I - 1, 1, 0)$ never exists in the deexcitation process because of the level order.

IV. ANGULAR MOMENTUM DEPENDENT MOMENTS OF INERTIA

It is a hard task for the theoretical work to reproduce the experimental excitation energy relative to a reference, $E^* - aI(I + 1)$ with $a = 0.0075 \text{ MeV}^{-1}$. By using Eq. (12) for E^* , we can make a crude estimation of A_x and j from the gradient of this curve as a function of I :

$$\frac{\partial[E_{\text{rot}}(I, 0, 0) - aI(I + 1)]}{\partial I} = 2(A_x - a)\left(I + \frac{1}{2}\right) - 2A_x j + \sqrt{pq}. \quad (36)$$

Most of the experimental curves shown by the dotted lines in Figs. 5 to 8, decrease monotonically with I , but they are a little bit convex upward. Therefore, regarding $A_x - a$ is negligibly small, we assume $A_x \sim a$, and get a gradient $-2aj + \sqrt{pq}$. If $j = 13/2$, the contribution of the first term is $-2aj \sim -0.097 \text{ MeV}$, but the gradient from the experimental curves is about -0.025 MeV for the positive parity bands, indicating $\sqrt{pq} \sim 0.072 \text{ MeV}$. Once the value of γ is fixed, the gradient depends on the value of j , so that larger j gives steeper gradient. The negative parity band TSD4 in ^{163}Lu has a steeper gradient than the other positive parity bands. If $\pi j_{15/2}$ is adopted for j , $-2aj + \sqrt{pq} \sim -0.11 + 0.072 \sim -0.04$, which agrees with the experimental value of -0.05 for the negative parity band TSD4 in ^{163}Lu . In ^{163}Lu , TSD4 band starts from $I = 47/2^-$ up to $83/2^-$. If $j = 15/2$ and $n_\beta = 0$ (the smallest value of n_β) are adopted, $R(= I - j)$ becomes even

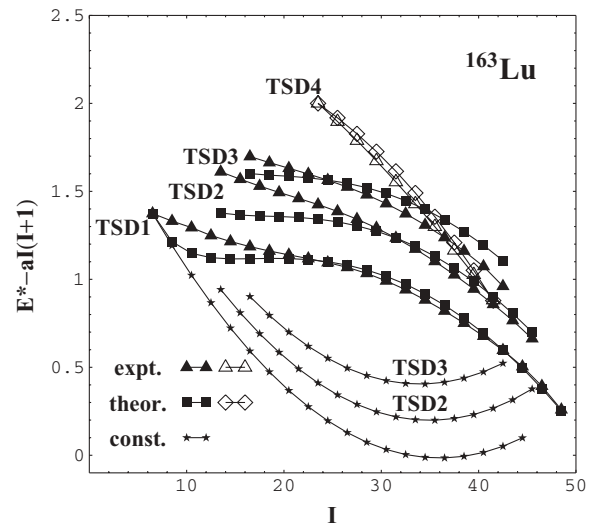


FIG. 5. The comparison between the experimental and the theoretical energy levels, $E^* - aI(I + 1)$ as functions of angular momentum I for ^{163}Lu . The vertical axis is in unit of MeV. For the positive parity bands, filled squares connected with solid lines indicate theoretical values, while filled triangles connected with dashed lines indicate experimental values. The stars connected with solid lines indicate the previous results with constant moments of inertia in I. For the negative parity band, open diamonds connected with solid lines indicate theoretical values, while open triangles connected with dashed lines indicate experimental values. The experimental data are from Refs. [2,3].

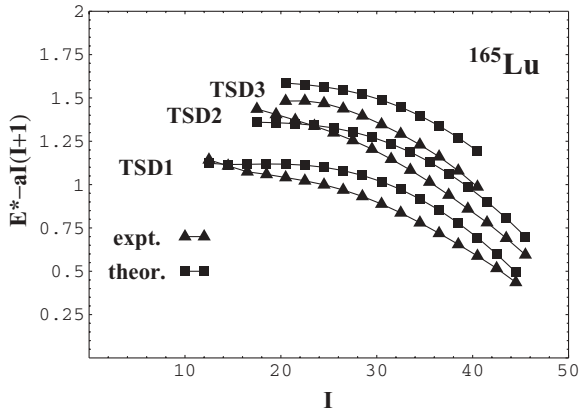


FIG. 6. The comparison between the experimental and the theoretical energy levels, $E^* - aI(I+1)$ as functions of angular momentum I for ^{165}Lu . The vertical axis is in unit of MeV. The meanings of the curves are as defined in Fig. 5. The experimental data are from Ref. [4].

and n_α takes an even value (see Eqs. (6) and (7)). Thus, TSD4 has precession quantum numbers (0,0). As for the negative parity band TSD3 in ^{167}Lu , we choose $\pi h_{11/2}$, as TSD3 in ^{167}Lu has a gradient similar to the other positive parity bands. In ^{167}Lu , TSD3 band starts from $I = 27/2^-$ up to $83/2^-$, and $R (= I - j)$ becomes even for $n_\beta = 0$, consequently TSD3 also has precession quantum numbers (0,0).

The excitation energy relative to a reference decreases with increasing I , and the dynamical moment of inertia increases with increasing angular frequency. These experimental results indicate there still remains the Coriolis antipairing (CAP) effect in the rotating core even in the TSD bands. As an attempt to reproduce the experimental energy curves, we simulate the effect of decreasing pairing on the moments of inertia in Eq. (3) simply by the replacement,

$$\mathcal{J}_0 \rightarrow \mathcal{J}_0 \frac{I - 0.69}{I + 23.5}. \quad (37)$$

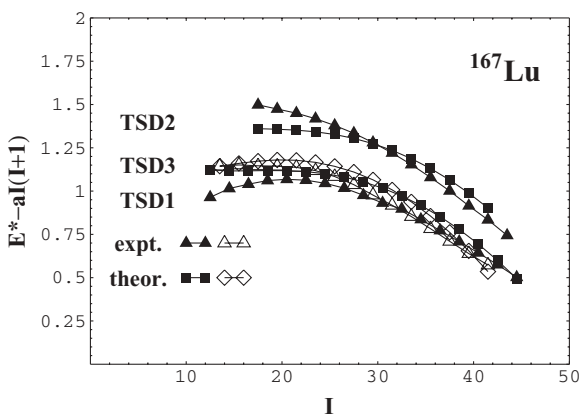


FIG. 7. The comparison between the experimental and the theoretical energy levels, $E^* - aI(I+1)$ as functions of angular momentum I for ^{167}Lu . The vertical axis is in unit of MeV. The meanings of the curves are as defined in Fig. 5. The experimental data are from Ref. [5].

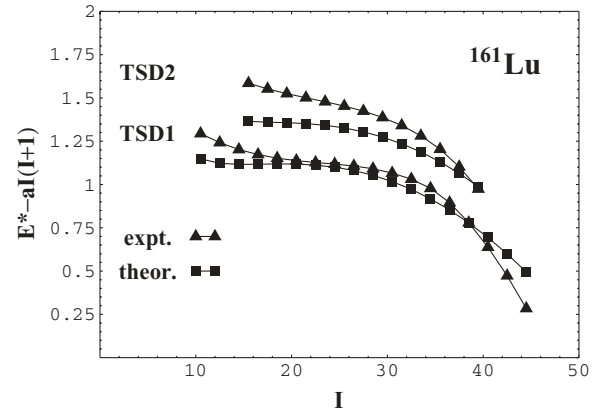


FIG. 8. The comparison between the experimental and the theoretical energy levels, $E^* - aI(I+1)$ as functions of angular momentum I for ^{161}Lu . The vertical axis is in unit of MeV. The meanings of the curves are as defined in Fig. 5. The experimental data are from Ref. [10].

For the positive parity bands, $\pi i_{13/2}$ orbital is assumed for the single-particle angular momentum j , while for the negative parity bands, $\pi j_{15/2}$ is assumed for ^{163}Lu and $\pi h_{11/2}$ for ^{167}Lu . The value of \mathcal{J}_0 is assumed to be 77.6 MeV^{-1} for the positive parity bands, and 81.6 MeV^{-1} for the negative parity bands. As for the positive parity bands, only the band-head energy of (0, 0) band is adjusted to the experimental band-head energy of TSD1 in ^{163}Lu , and nothing is adjusted over the isotopes. The value of $\gamma = 17^\circ$ and $V = 2.6 \text{ MeV}$ are fixed. Adopting these parameters, we carried out exact diagonalization of the total Hamiltonian with \mathcal{J}^{rig} on the D_2 -invariant basis in Eq. (5) to obtain the energy levels for a given I . The precession quantum numbers can be assigned without ambiguity to the theoretical TSD bands in comparison with the algebraic solution, whose accuracy has been demonstrated in I.

As for negative parity bands, the band-head energy of (0, 0) band is adjusted to the experimental band-head energy in each of $^{163,167}\text{Lu}$. In Figs. 5 to 8, we compare theoretical energy levels of $E^* - aI(I+1)$ with experimental ones. In these figures, theoretical values are shown as filled squares for positive-parity bands and open diamonds for negative-parity bands connected by solid lines, while experimental values as filled triangles for positive-parity bands and open triangles for negative-parity bands connected by dashed lines. In Fig. 5, for the sake of comparison, we add three curves for TSD1, 2 and 3 of ^{163}Lu (the stars connected with solid lines), which are calculated with the same constant moments of inertia as adopted in I ($\mathcal{J}_0 = 52.4 \text{ MeV}^{-1}$ and $s = 120$). It is clearly seen that the substantial improvement is attained by the inclusion of angular momentum dependence for moments of inertia. Quite good fits to the experimental data are obtained over isotopes.

By the crude estimation in Eqs. (14a) and (14b), we have seen that $(\Delta E_2 - \Delta E_1) - \Delta E_1 = -(A_y + A_z) < 0$. Thus, $\Delta E_2 - \Delta E_1$ corresponding to the energy difference between TSD3 and TSD2 is expected to be less than the energy difference between TSD2 and TSD1 (ΔE_1). The exact results also reproduce such an inequality, which is confirmed experimentally as seen in Figs. 5 and 6. It is an interesting feature that

all the positive parity TSD band levels are well reproduced in terms of a common \mathcal{J}^{rig} over the isotopes $^{161,163,165,167}\text{Lu}$. This suggests that additional pairs of neutron take part in the superfluidity. Such a mechanism gives rise to the CAP effect, which should be interpreted in terms of microscopic formalism. As for the negative parity band, a larger \mathcal{J}_0 value is needed to reproduce the experimental energy curve, implying that the valence proton in different orbital may cause different core polarization effect. This problem is also beyond a scope of our macroscopic formalism.

V. CONCLUSION

The selection rules are inferred from the lowest order overlaps between the original Holstein-Primakoff boson states and the quasiboson states in which the total Hamiltonian is diagonalized. The algebraic expressions for B values under the “ $\Delta n = 0$ ” approximation are expressed in terms of the factor $1/I$ and the nondiagonal elements of the overlap coefficient G depending on the precession quantum numbers. These simple expressions for B values enable us to lead their relations between the various transitions among TSD bands, which are proved to be consistent with existing experimental data. Such theoretical expressions for B values can help to identify the observed TSD bands whose angular momenta are not yet determined.

The algebraic formula for the simplified case of $V = 0$ is useful to get crude physical ideas. For example, it provides the

energy level scheme over the TSD bands, predicting a measure of anharmonicity, and contributes to guess the values of j and A_x . It also elucidates the effect of Coriolis and recoil terms caused by the valence nucleon on the transition rates through the overlap coefficient G . Although the quantum numbers for the yrast favored and unfavored bands are common both for rigid-body and hydrodynamical moments of inertia, the level scheme is different between two cases. Consequently, different transition schemes come out.

We have extended the particle-rotor model including an angular momentum dependence for moments of inertia, which simulates the collapse of pairing correlation in the rotating core. This method is applied to the odd- A isotopes $^{161,163,165,167}\text{Lu}$, as realistic examples. The particle-rotor Hamiltonian with the rigid-body moments of inertia and with only one set of parameters reproduces overall trends of the energy spectra along the triaxial, strongly deformed (TSD) rotational bands in four odd- A nuclei, i.e., TSD1, TSD2, TSD3, and TSD4 in ^{163}Lu ; TSD1, TSD2, and TSD3 in ^{165}Lu ; and TSD1 and TSD2 in ^{167}Lu and ^{161}Lu . As for the positive parity bands, a valence proton occupies $i_{13/2}$ orbital, while for the negative parity bands the proton is assumed to occupy $j_{15/2}$ orbital in ^{163}Lu and $h_{11/2}$ orbital in ^{167}Lu . Based on the calculations with the rigid-body moments of inertia, we find that preferable assignments of quantum numbers are $(n_\alpha, n_\beta) = (0, 0)$ for TSD1 in $^{161,163,165,167}\text{Lu}$, $(1, 0)$ for TSD2 in $^{161,163,165,167}\text{Lu}$, $(2, 0)$ for TSD3 in $^{163,165}\text{Lu}$, and for the negative parity band $(0, 0)$ for TSD4 in ^{163}Lu and TSD3 in ^{167}Lu .

-
- [1] K. Tanabe and K. Sugawara-Tanabe, Phys. Rev. C **73**, 034305 (2006); **75**, 059903(E) (2007).
 - [2] S. W. Ødegård *et al.*, Phys. Rev. Lett. **86**, 5866 (2001).
 - [3] D. R. Jensen *et al.*, Phys. Rev. Lett. **89**, 142503 (2002).
 - [4] G. Schönwaßer *et al.*, Phys. Lett. **B552**, 9 (2003).
 - [5] H. Amro *et al.*, Phys. Rev. C **71**, 011302(R) (2005).
 - [6] K. Tanabe and K. Sugawara-Tanabe, Phys. Lett. **B34**, 575 (1971).
 - [7] A. Bohr, Mat. Fys. Medd. K. Dan. Vidensk. Selsk. **26**, no.14 (1952).
 - [8] I. Hamamoto, Phys. Rev. C **65**, 044305 (2002).
 - [9] G. B. Hagemann, Eur. Phys. J. A **20**, 183 (2004).
 - [10] P. Bringel *et al.*, Phys. Rev. C **73**, 054314 (2006).
 - [11] G. Schönwaßer *et al.*, Nucl. Phys. **A735**, 393 (2004).
 - [12] A. Bohr and B. R. Mottelson, *Nuclear Structure* (Benjamin, Reading, MA, 1975), Vol. II, Chap. 4.
 - [13] K. Tanabe, J. Math. Phys. **14**, 618 (1973).
 - [14] K. Sugawara-Tanabe and K. Tanabe, Nucl. Phys. **A208**, 317 (1973).
 - [15] K. Tanabe, K. Enami, and N. Yoshinaga, Phys. Rev. C **59**, 2494 (1999).